OPEN

During Cycling What Limits Maximum Mechanical Power Output at Cadences above 120 rpm?

EMMA F. HODSON-TOLE[1], OLLIE M. BLAKE[2], and JAMES M. WAKELING[2]

[1]*Musculoskeletal Science and Sports Medicine Research Centre, Manchester Metropolitan University, Manchester, UNITED KINGDOM; and* [2]*Department of Biomedical Physiology and Kinesiology, Simon Fraser University, Burnaby, British Columbia, CANADA*

ABSTRACT

HODSON-TOLE, E. F., O. M. BLAKE, and J. M. WAKELING. During Cycling What Limits Maximum Mechanical Power Output at Cadences above 120 rpm? *Med. Sci. Sports Exerc.*, Vol. 52, No. 1, pp. 214–224, 2020. **Purpose:** A key determinant of muscle coordination and maximum power output during cycling is pedaling cadence. During cycling, the neuromuscular system may select from numerous solutions that solve the task demands while producing the same result. For more challenging tasks, fewer solutions will be available. Changes in the variability of individual muscle excitations (EMG) and multimuscle coordination, quantified by entropic half-life (EnHL), can reflect the number of solutions available at each system level. We, therefore, ask whether reduced variability in muscle coordination patterns occur at critical cadences and if they coincide with reduced variability in excitations of individual muscles. **Methods:** Eleven trained cyclists completed an array of cadence–power output conditions. The EnHL of EMG intensity recorded from 10 leg muscles and EnHL of principal components describing muscle coordination were calculated. Multivariate adaptive regressive splines were used to determine the relationships between each EnHL and cycling condition or excitation characteristics (duration, duty cycle). **Results:** Muscle coordination became more persistent at cadences up to 120 rpm, indicated by increasing EnHL values. Changes in EnHL at the level of the individual muscles differed from the changes in muscle coordination EnHL, with longer EnHL occurring at the slowest (<80 rpm) and fastest (>120 rpm) cadences. The EnHL of the main power producing muscles, however, reached a minimum by 80 rpm and did not change across the faster cadences studied. **Conclusions:** Muscle coordination patterns, rather than the contribution of individual muscles, are key to power production at faster cadences in trained cyclists. Reductions in maximum power output at cadences above 120 rpm could be a function of the time available to coordinate orientation and transfer of forces to the pedals. **Key Words:** SKELETAL MUSCLE, SAMPLE ENTROPY, LOCOMOTION, ELECTROMYOGRAPHY, COORDINATION, PEDALING

When a human pedals on a bicycle, appropriate joint actions and coordination across the multiple limb segments must occur to generate the required movement patterns and reaction forces at the pedal. Activity across multiple muscles in the leg is, therefore, required (1), with timing and coordination between muscles critical factors in determining power output and efficiency (2).

One of the key determinants of muscle coordination and movement efficiency during cycling is pedaling cadence. Ninety revolutions per minute has been suggested to be an optimal cadence for delaying neuromuscular fatigue (3) and has been related to minimization of muscle forces, stress, and activation during cycling (4). Long distance, endurance trained athletes tend to have a preferred pedaling cadence between 85 and 95 rpm (5,6). In contrast, maximum power output is achieved when pedaling at cadences between 110 and 120 rpm (7–10), close to the cadences often observed in track cyclists completing shorter distance, power-based events (e.g., 110–135 rpm team pursuit Fig. 1 in (11)). Interestingly, cadences above 120 rpm are associated with a wide range of changes spanning features of force application, multimuscle coordination, and excitation patterns of individual muscles all of which reduce maximum power output.

At the individual muscle level, cadences faster than 120 rpm are related to increased excitation (2,12) and constant burst

Address for correspondence: Emma F. Hodson-Tole, Ph.D., Department of Life Sciences, Manchester Metropolitan University, Manchester, M1 5GD, United Kingdom; E-mail: e.tole@mmu.ac.uk.

Submitted for publication February 2019.
Accepted for publication July 2019.
Supplemental digital content is available for this article. Direct URL citations appear in the printed text and are provided in the HTML and PDF versions of this article on the journal's Web site (www.acsm-msse.org).

0195-9131/20/5201-0214/0
MEDICINE & SCIENCE IN SPORTS & EXERCISE®

DOI: 10.1249/MSS.0000000000002096

durations that, coupled with the shorter pedal cycle durations, result in longer duty cycles (2). In some muscles cadences above 120 rpm also lead to preferential recruitment of faster motor unit populations (13,14) and early derecruitment of slower motor unit populations in each excitation burst (15). These factors seem important for force production, particularly at very high cadences (16,17), and for forces to be produced efficiently under such conditions (18). At the level of the whole limb, efficiency is seen to reduce beyond cadences of 120–140 rpm, whereas reductions in the variability of muscle coordination patterns suggest limitations in coordination begin to occur (2). The net effect of these changes, from a mechanical perspective, is an increase in the ineffective forces applied to the pedals (2). Distinct changes in behavior are, therefore, apparent at different levels of the nervous and musculoskeletal systems, which taken together reduce the power output that can be generated within the constraint of shorter pedal cycle durations.

For any motor task the neuromuscular system may select from a number of solutions that are available to solve the task, all of which provide the same result (19). Within the context of this manuscript we consider that solutions can be flexible (i.e., there may be more or better solutions for a given task), and to encapsulate this will use the phrase "solutions available." The influence of cadence on maximum power output suggests that the solutions available within the musculoskeletal system that can meet the task demand is constrained by pedal cycle duration. It is not known, however, whether such limitations predominantly occur at the level of the whole limb (i.e., multimuscle coordination patterns) or at the level of individual muscles. It is likely there are fewer muscles in the human leg than there are motor units within any one of the leg muscles. Therefore, the limb as a whole will have fewer solutions available to meet the demands of cycling exercise than will an individual muscle. However, although individual muscles will comprise hundreds of motor units, those units are unlikely to operate independently. The solutions available within a muscle may, therefore, be constrained by several factors. For example: organization into motor unit task groups (20); common neural drive acting across motor unit populations (21) and; spatial organization of motor units influencing which can appropriately contribute to the direction of the force vector required at the joint (22–24). As such, it may be that although the number of solutions available to the limb as a whole is limited by pedal cycle duration, reductions in the solutions available within individual muscles may not occur. We, therefore, ask whether fewer solutions in the muscle coordination patterns are linked to fewer solutions in the excitation patterns of individual muscles, or whether fewer solutions in muscle coordination patterns occur even when the number of solutions available within individual muscle excitation patterns is not reduced.

One way in which changes in the solutions available within a system may be observed is by using entropy-based nonlinear analyses, to quantify the time-scale over which a given signal structure persists (25–27). This calculation involves reshaping the original time series (e.g., intensity envelope of an EMG signal) at increasing time intervals and quantifying the structure of each newly created signal using sample entropy (SampEn) (27) (Fig. 1). Typically, EMG signals have a high degree of structure resulting in a low SampEn value (Fig. 1 here, and see Fig. 1 in (28)); but the structure is dissipated during the reshaping process resulting in greater SampEn values that plateau as the signal is completely randomized (25,28,29). Normalizing SampEn values to the maximum obtained and identifying the time interval, where SampEn = 0.5, identifies the time-scale at which the signal loses structure and transitions to being random (i.e., the time-scale over which structure has persisted) and is termed the entropic half-life (EnHL) (27) (Fig. 1).

Evaluation of the features that shape EMG signals and their effects on EnHL have been conducted using both simulated (28) and physiological EMG (28,29). Entropic half-life reveals persistent and nonrandom structure in raw EMG signals, the intensity envelopes of those signals, and in the multimuscle coordination patterns. In the raw EMG, this structure represents motor unit action potential shape, firing rate variability (or lack of) and coherence between motor units (29). The EnHL of EMG intensities is generally longer than in the raw signals, indicating greater and more persistent structure that reflects smoothing of time-dependent fluctuations. Fluctuations in burst parameters (e.g., burst duration and duty cycle), therefore, likely dominate the structure of EMG intensity signals (28,29). The EnHL of the EMG intensity are, however, typically an order of magnitude shorter than the EMG burst duration, indicating that information pertaining to fluctuations in motor unit firing statistic persist within the intensity envelope (28,29). These fluctuations in firing statistics are more rapid than the duration of the excitation and are, therefore, not limited by excitation duration, although it is evident that interactions exist (28,29).

As multimuscle coordination patterns represent the net behavior of all recorded muscles, they contain information on the modulation of excitation across synergistic groups over the movement cycle. Fluctuations in the interactions between synergistic excitations will influence structure persistence in muscle coordination. The more muscles amalgamated within the analysis the more ways in which coordination can vary and dissipate structure. Accordingly, EnHL of multimuscle coordination patterns are shorter (less persistent structure) than for the individual EMG intensities, but are still influenced by fluctuations in burst duration and duty cycle (29). Entropic half-life, therefore, provides means of moving beyond instantaneous measures of excitation. The number of solutions available to the motor control system will influence fluctuations and persistence of structure at all signal levels that EnHL can quantify to reflect repeating interactions between constituent motor unit action potential characteristics, synergistic excitation, and EMG burst parameter fluctuations.

Entropic half-life has previously been used to show that the time-scales over which muscle coordination patterns persist increases for cycling at high loads (25). This suggests there

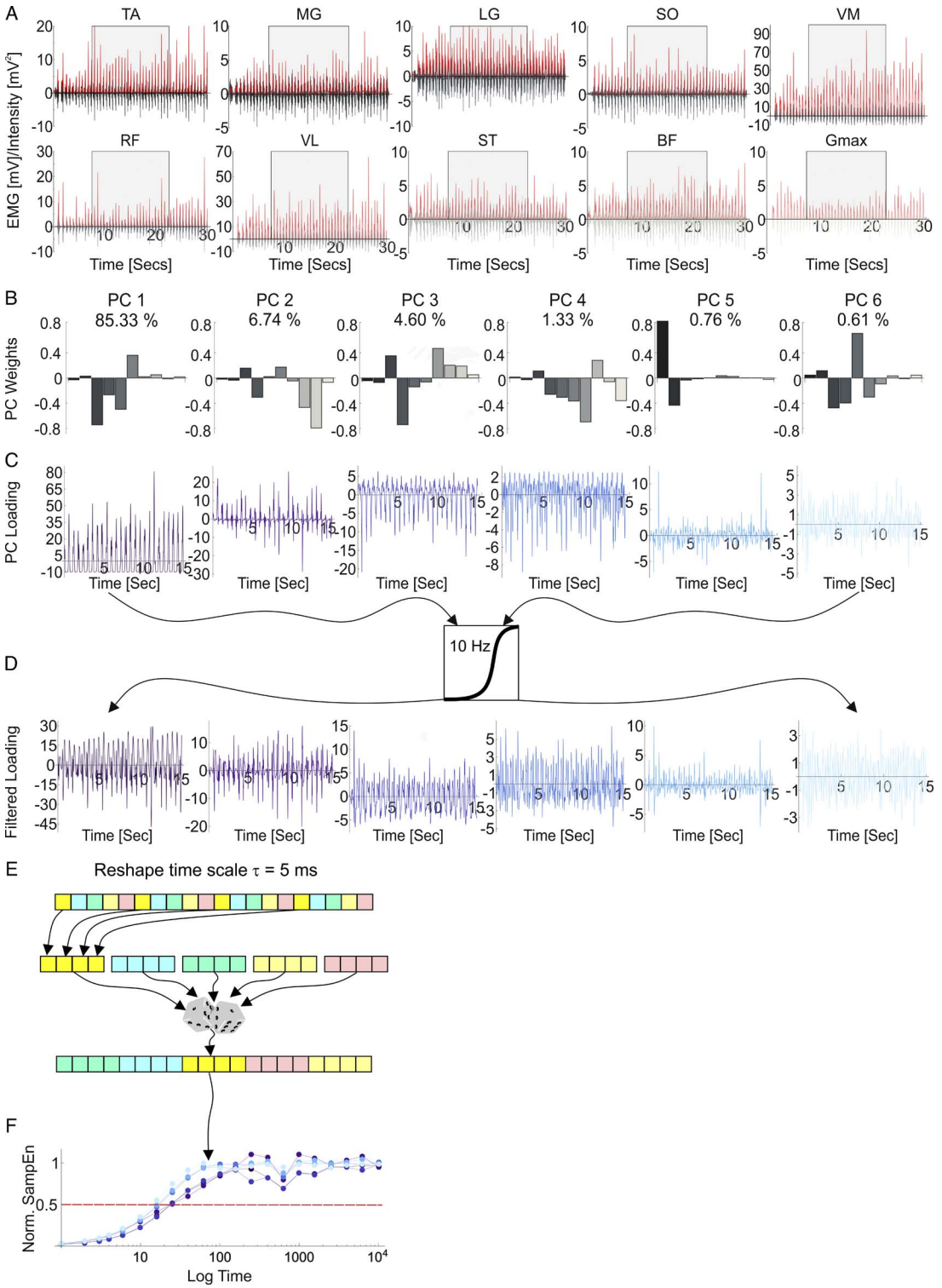

FIGURE 1—Overview of data analysis process. A, EMG intensity envelopes (red-scale) were calculated from the raw EMG (grayscale) recorded from the 10 lower leg muscles. A 15-s epoch (shaded block) of steady cycling was selected to form a 10 muscles × 15,000 data point (15 s at 1000 Hz) matrix for principal component analysis. The PCA provided the weighting of each muscle within a coordination pattern (B) and how much of that coordination pattern contributed to the total signal at any given time point (loading, (C)). For each muscle coordination pattern (B) each bar represents the contribution of an individual muscle to the coordination pattern and the bars are ordered to match the sequence of muscles in A, TA through to Gmax. The first PCs explain the largest proportion of the variance (denoted above each weighting). The resulting loading scores were high pass filtered (D) and standardized before being reorganized over different time scales (a single 5-ms time scale is represented, (E)). Sample entropy of each reshaped signal is calculated and normalized to SampEn of a random permutation of the signal, meaning values span from structured (low SampEn) to completely random (high SampEn) when plotted as a function of the reshape-scales (F). The time at which normalized SampEn = 0.5 (*red horizontal line*) represents the time over which structure persisted in the coordination pattern. The same filtering and reshape/SampEn process was applied to the EMG intensity envelopes (A). Data shown are from one trial from one participant.

are fewer solutions available within muscle coordination that meet the increased load demand. The work, however, only included one cycling cadence (90 rpm). When cadences spanning 60 to 140 rpm were studied, EnHL of muscle coordination increased at faster cadences, whereas EnHL of EMG intensity of individual muscles decreased (29). These experiments, however, only included a single, low load (6.5 N·m). Given the potential importance of 120 rpm in terms of changes in force application, multimuscle coordination, and excitation patterns of individual muscles, the range of cadences included was also not wide enough to fully reveal how the underlying control processes, across muscle coordination, and individual muscle excitation characteristics respond to different load and cadence demands.

We, therefore, predicted that patterns in muscle coordination will become more persistent at faster cadences, represented by longer EnHL values. In addition, we predict that changes in EnHL at the level of the individual muscles will differ from the changes in muscle coordination EnHL, with no change or shorter EnHL occurring at faster cadences. In addition, we predict that 120 rpm will be a critical cadence at which changes in EnHL values of both muscle coordination and individual muscle excitation characteristics will occur.

METHODS

Data acquisition. Details of data collection have been reported in previous work (2) and so will be briefly described here. Eleven male cyclists (mean ± SE age, 33.9 ± 3.1 yr; mass, 72.8 ± 2.1 kg; height, 179.1 ± 1.9 cm), all of whom were competitively trained (mean ± SE cycling distance per year: 10,773 ± 1575 km), gave informed written consent to participate in the study, which was approved by the local ethics committee conducted in accordance with the Office of Research Ethics at Simon Fraser University.

The cycling protocol comprised cadences ranging between 40 and 180 rpm, at 20 rpm intervals, each of which were completed at 100, 200, 300, and 400 W on an indoor cycle trainer (Schoberer Rad Messtechnik, Jülich, Germany). The geometry of the cycle trainer was adjusted to match, as closely as possible, the geometry of the participant's bike and participants used their own clipless pedals and shoes. During a 10-min warm-up participants cycled for 5 min at 100 W followed by 5 min increasing 20 $W \cdot min^{-1}$, all at their chosen cadence. Participants pedaled at all cadences (randomized order) within a randomly selected power condition, before each cadence was repeated for a new, randomly selected, power condition. Each trial was 30 s long, during which time participants were instructed to remain seated with their hands on the brake hoods. Ninety seconds rest was provided between trials.

EMG signals were recorded from 10 muscles [*Gastrocnemius lateralis* (LG), *soleus* (SO), *Gastrocnemius medialis* (MG), *Tibialis anterior* (TA), *Vastus lateralis* (VL), *Rectus femoris* (RF), *Vastus medialis* (VM), *Biceps femoris* (BF), *Semitendinosus* (ST), and *Gluteus maximus* (GMax)] of the right leg of each participant (Fig. 1A). Signals were recorded (2000 Hz, 16 bit analog-to-digital converter USB-6210; National Instruments, Austin, TX) from bipolar Ag/AgCL surface electrodes (10 mm diameter, 21 mm interelectrode distance; Norotrode, Myotronics, Kent, WA) after being amplified (×1000) and band pass filtered (10–500 Hz). A pedal switch output identified top-dead center of the crank cycle and was simultaneously recorded with EMG signals.

Data analysis. Recorded EMG signals were resolved into their intensities in time–frequency space using a filter bank of 11 wavelets ($0 \le k \le 10$) (30) (Fig. 1A). The total intensity was calculated as the sum of intensities from wavelets k = 1–10 (frequency bandwidth of ~11–432 Hz) to provide a representation of the power of the EMG signal at each time point (30). The intensities were normalized to the mean for each muscle for each participant across trials. Activation burst duration was calculated as the duration that intensity was greater than 5% of the maximum for each pedal cycle, whereas duty cycle was the proportion of this value in relation to the pedal cycle duration. Prior to calculation of EnHL, a 15-s epoch of steady state cycling was selected from the normalized intensities (Fig. 1A), resampled to 1000 Hz, high pass filtered (Butterworth 10 Hz cut-off), to remove the temporal bursting component of pedal cycles, and standardized to have a mean of zero and standard deviation of one.

Calculation of EnHL involved: (i) resampling the standardized signals for reshape scales spanning 1 to 10,000 ms (27) (Fig. 1E); and (ii) calculating the SampEn (m, r, N) of each resampled time series using a freely available software package (31). The reshape-scale process reorganizes the signal over multiple time scales (number of data points), enabling the time scale over which data points remain affiliated to each other to be evaluated. SampEn quantifies the degree of similarity in a signal of length N (here N = 15,000), based on the conditional probability that two sequences or patterns of m consecutive data points, similar to each other with tolerance equal to r, will remain similar when a consecutive data point is added (m + 1) (32). Values of m = 0 (interpreted as the negative logarithm of the probability of a match of length 1 (31)) and m = 1 with r = 0.2 were applied. The SampEn values for m = 1 were normalized to those corresponding to m = 0 (representing SampEn for a random permutation of the signal), effectively normalizing values so they spanned structured to completely random (25). When these normalized SampEn values are plotted as function of the reshape-scales (Fig. 1F), the time scale at which SampEn = 0.5 represents the time over which structure persisted in the EMG intensity envelope, and is termed EnHL (27).

In addition to determining structure of the EMG intensity envelopes from individual muscles, we also wished to quantify structure across the muscle coordination patterns. Muscle coordination within each trial was, therefore, calculated from the normalized, wavelet-derived intensities of the 10 muscle EMG using principal component analysis (33) (Fig. 1B–C). Matrix $\boldsymbol{A}$ of dimensions $P \times N$ (P = 10 muscles, N = 15,000; 15 s at the 1000-Hz sample rate) was constructed, and the mean intensity for each muscle subtracted before the covariance matrix $\boldsymbol{B}$ was calculated. Eigenanalysis of $\boldsymbol{B}$ provided the principal

components of $\boldsymbol{A}$, with the loading scores given from $\xi'\boldsymbol{A}$, where ξ' are the transpose of the eigenvectors of $\boldsymbol{B}$. Each principal component, therefore, reveals the weighting of each muscle within a coordination pattern (Fig. 1B). The highest principal components explain the largest proportion of the variance in $\boldsymbol{A}$, and the loading score of each component reveals how much of that coordination pattern contributed to the total signal at any given time point. A time series from each trial was constructed from the time-varying loading scores of each principal component (Fig. 1C) and the EnHL for each was calculated, as described above, enabling the time-scale over which structure persisted in the variability of the muscle coordination patterns to be determined.

To ensure that the EnHL values could be interpreted as representing physiologically related structure within the signal (i.e., signal content that fluctuates in a time-dependent, nonrandom manner), we compared them with values obtained from analysis of phase randomized surrogates of the EMG intensity envelope for each muscle and trial. This process removes the structure encoded in the phase of the signal and structure related to EMG bursting patterns, motor unit firing, and shape of individual action potentials (29), but maintains the signal's power spectrum.

Statistical analysis. Multivariate adaptive regressive splines (MARS) (34) were used to determine the relationships between each EnHL and cycling condition or excitation characteristics, implemented using the "earth" package (35) in R 3.3.1 (R Core Team 2018). Multivariate adaptive regressive splines is a flexible, nonparametric regression technique that enables different subregions within the data set to be described based on the addition and interaction of contributing variables. It derives a set of basis functions comprising: (i) an intercept; (ii) a hinge function, of the form $\max(0, |c - x|)$ that splits these data into subregions; and (iii) a product of two or more hinge functions, modeling interactions between variables. This analysis approach was chosen as the hinge functions (which are automatically determined by the data set (34)) quantify transition points where the relationship between variables changes. For example, we could, therefore, determine whether nonlinear changes in EnHL occurred as a function of cycling cadence and crank torque, and whether the nonlinearity hinged around critical cadence or crank torque values.

To quantify the relationship between cycle condition and the EnHL of muscle coordination, the median EnHL of each PC was calculated from the group data. This approach removed potential correlations within the data due to the repeated measures experimental protocol, and also reduced the potential for outliers that can influence the MARS analysis (34). The cycling condition associated with each EnHL were used to provide a model, predicting EnHL as a function of cadence and crank torque (with interactions between the two permitted). Crank torque was used, rather than power, to account for the use of cadence as the other variable. For the EnHL of individual muscle excitation patterns and the phase randomized surrogate signals, a similar process was completed. In addition, to identify the effect of cycling condition, the relationship between excitation duration and duty cycle (and their interaction) with EnHL was also determined.

RESULTS

EnHL of muscle coordination. The first six principal components explained over 98% of the variance across muscle EMG intensity patterns (Table 1). The EnHL for the loading scores of the principal components, representing muscle coordination, are shown in Figure 2, Supplemental Digital Content 1 (animated rotation of plots in Fig. 2, providing multiple perspectives of the three-dimensional (3D) space, http://links.lww.com/MSS/B704) and Supplemental Digital Content 2 (animated rotation of data in Fig. 2, including interquartile ranges of the data set, http://links.lww.com/MSS/B705). The results of the related MARS analysis are shown in Table 1. Except at the very slowest cadence, the longest EnHL occurred in the first two principal components. These first two components were characterized by increasing EnHL (fewer fluctuations/increased persistence in structure) from the slow to faster cadences, that MARS analysis identified reached a maximum at 120 rpm and remained approximately constant (PCI ~21 ms and PCII ~18–20 ms) at faster cadences. In contrast, the EnHL of PCIII increased from 40 to 80 rpm, remained approximately constant (~15 ms) between 80 and 120 rpm and declined (greater fluctuations/decreased persistence in structure) at cadences faster than 120 rpm. The lower principal components were approximately constant at slower cadences (~13–15 ms) and became shorter at cadences above 80 to 100 rpm. In each of the principal components, the interquartile ranges were small and consistent across data points (Supplemental Digital Content 2, animated rotation of data in Fig. 2, including interquartile ranges of the data set, http://links.lww.com/MSS/B705), indicating that the MARS fit to the median values is representative of the group behavior.

Crank torque had an effect on EnHL of PCII and PCIV–PCVI, with MARS analysis identifying 23.87 N·m being the hinge point for all the components except PCVI where 28.64 N·m was the hinge, although the MARS model fit was low for this component (r^2 = 0.52, Table 1). Across

TABLE 1. Details of principal component characteristics and MARS models fit to these data as a function of cycling cadence (cad) and torque.

PC	Variance Explained [IQR] (%)	MARS Model	Model Fit (r^2)
I	36.61 [6.21]	20.59 – (0.11 × Max [0,120 – cad])	0.91
II	25.48 [4.75]	19.12 – (0.07 × Max [0,120 – cad]) – (0.09×Max [0,23.87 – torque]) – (0.05×Max [0,torque – 23.87])	0.84
III	12.32 [2.90]	14.90 – (0.07 × Max [0,80 – cad]) – (0.09×Max [0,cad – 120])	0.80
IV	7.99 [2.14]	13.39 – (0.10 × Max [0,cad – 100]) – (0.04×Max [0,torque – 23.87]) – (0.0005×Max [0,cad×torque – 1909.61])	0.82
V	5.24 [1.58]	11.59 – (0.05 × Max [0,cad – 100]) + (0.10×Max [0,23.87 – torque]) – (0.03×Max [0,torque – 23.87])	0.67
VI	3.65 [0.97]	11.13 – (0.03 × Max [0,cad – 80]) + (0.08×Max [0,28.64 – torque]) – (0.03×Max [0,torque – 28.64])	0.52

IQR indicates interquartile range of the median variance explained across the data set.

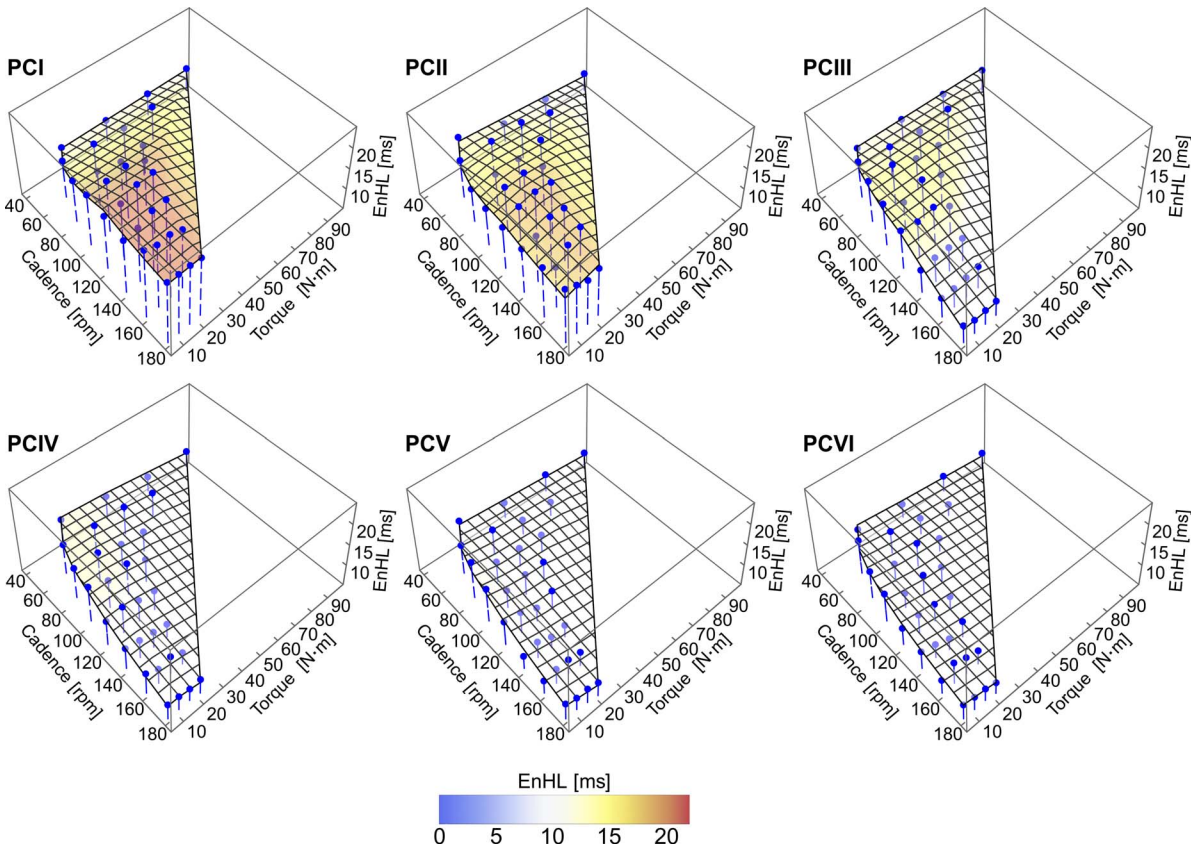

FIGURE 2—EnHL values for the first six principal components recorded for each cadence–crank torque cycling condition (*blue points*). The overlaid surface represents the principal component EnHL values predicted as a function of cadence and torque by MARS analysis. Equations for the surface and associated goodness of fit values are provided in Table 1. See Supplemental Digital Content 1 for animations of the graphics rotating through different viewpoints, http://links.lww.com/MSS/B704 and Supplemental Digital Content 2 for animations of the graphics including data points indicating the group inter-quartile ranges, http://links.lww.com/MSS/B705.

PCIV–PCVI, there was an interaction effect between cadence and crank torque that did not occur in PCII.

EnHL in individual muscle excitation. The EnHL of each individual muscle excitation pattern and the phase randomized surrogate as a function of cadence and crank torque is shown in Figure 3, Supplemental Digital Content 3 (animated rotation of plots in Fig. 3, providing multiple perspectives of the 3D space, http://links.lww.com/MSS/B706) and Supplemental Digital Content 4 (animated rotation of data in Fig. 3, including interquartile ranges of the data set, http://links.lww.com/MSS/B707). In all muscles, the EnHL values for the surrogate signal were significantly lower (greater fluctuations/decreased persistence in structure) than EnHL of the physiological signals (mean ± SD: surrogate EnHL, 6.84 ± 1.06 ms; EMG intensity EnHL, 23.14 ± 5.61 ms; Wilcoxon Signed Rank Test $P < 0.001$) and EnHL of surrogate signals changed very little with cycle condition (mean ± SD difference between minimum and maximum values, 0.85 ± 0.25 ms).

Across all the muscles, the longest EMG intensity EnHL occurred at the slowest cadences and lowest crank torques (Fig. 3, Supplemental Digital Content 3 animated rotation of plots in Fig. 3 providing multiple perspectives of the 3D space, http://links.lww.com/MSS/B706, Supplemental Digital Content 4 animated rotation of data in Fig. 3, including interquartile ranges of the data set, http://links.lww.com/MSS/B707). The longest EnHL were recorded in VM (48.58 ms) and VL (53.46 ms) (fewest fluctuations/greatest persistence in structure). In each muscle, except soleus, the MARS model included a hinge point related to cadence. In these muscles, EnHL decreased (greater fluctuations/decreased persistence in structure) from the slowest pedaling cadence until 80 rpm, except BF where EnHL continued to decrease until 100 rpm. The EnHL in TA, VM, and VL plateaued after 80 rpm (14.78 ms, 17.60 ms, 17.82 ms, respectively), with no further change occurring as a function of cadence. In the other muscles (MG, LG, RF, BF, GMax), EnHL increased from 120 rpm across faster cadences. In seven of the muscles, MARS analysis identified a hinge function related to crank torque, either at 23.87 N·m (BF) or 28.65 N·m (TA, MG, LG, SO, VL, ST). In RF and GMax, an interaction between cadence and crank torque was also identified by the model (Table 2). In all muscles, except RF and GMax, the interquartile range of the group data was quite small (Supplemental Digital Content 4, animated rotation of data in Fig. 3, including interquartile ranges of the data set, http://links.lww.com/MSS/B707). More variability in the data set were apparent at the extreme cadences, with very large differences occurring in RF and GMax at the lowest power (100 W) fastest cadence (180 rpm) condition.

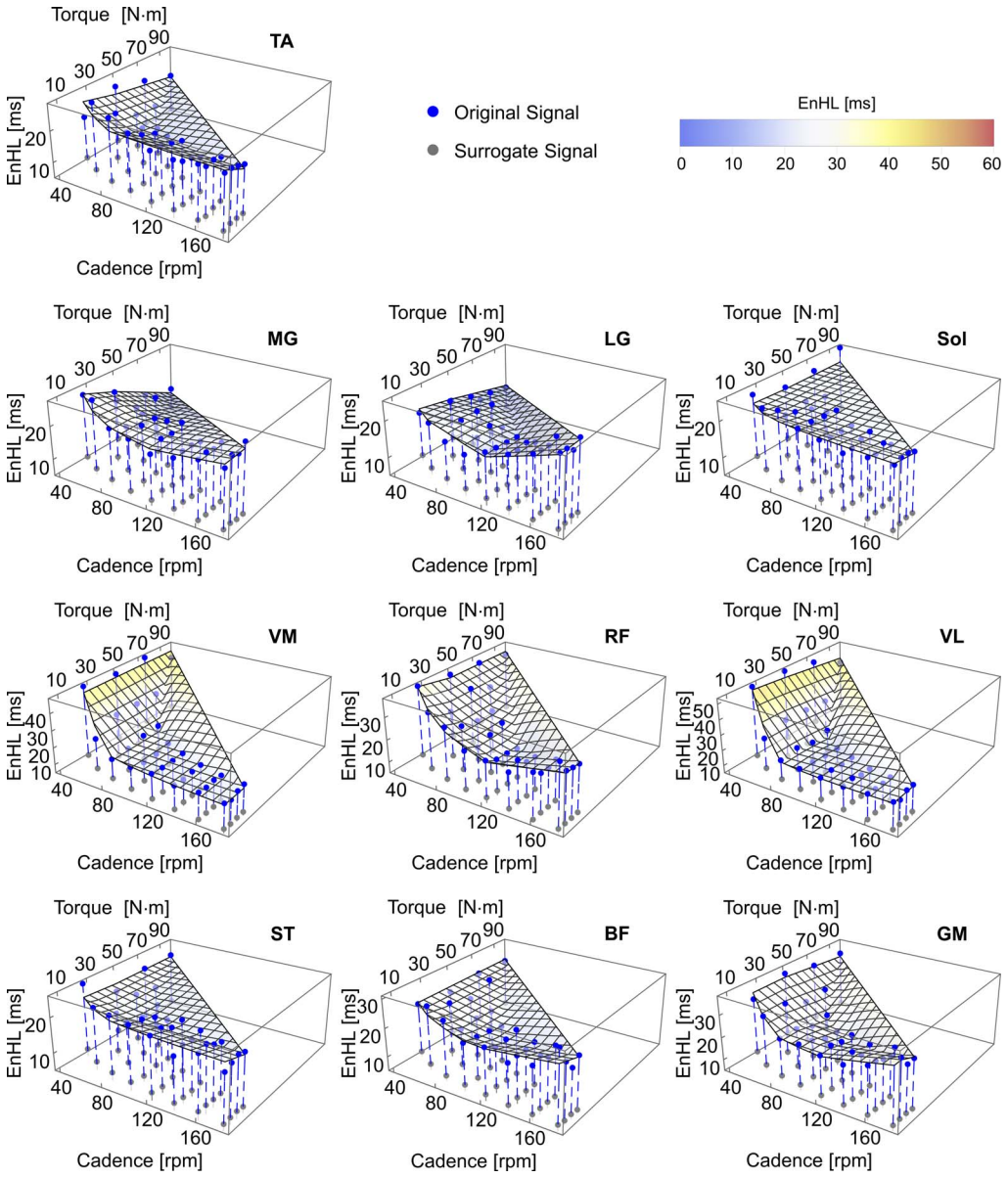

FIGURE 3—EnHL values for excitation patterns (*blue points*) and phase randomized surrogate signals (*gray points*) of individual muscles recorded for each cadence–crank torque cycling condition. The overlaid surface represents the excitation pattern EnHL values predicted as a function of cadence and torque by MARS analysis. Equations for the surface and associated goodness of fit values are provided in Table 2. See Supplemental Digital Content 3 for animations of the graphics rotating through different viewpoints, http://links.lww.com/MSS/B706 and Supplemental Digital Content 4 for animations of the graphics including data points indicating the group inter-quartile ranges, http://links.lww.com/MSS/B707.

Overall, for the midrange cadences (i.e., 80–160 rpm) variation was small, indicating that the MARS fit to the median values is representative of the data set.

The EnHL of each individual muscle as a function of excitation burst duration and duty cycle is shown in Figure 4 and Supplemental Digital Content 5 (animated rotation of plots

TABLE 2. Details of the MARS model of EnHL as a function of cadence (cad) and torque, in each of the 10 lower leg muscles analyzed.

Muscle	MARS Model	Model Fit (r^2)
Tibialis anterior	18.39 + (0.14 × Max [0,80 – cad]) + (0.26 × Max [0,28.65 – torque]) – (0.08× Max [0,torque – 28.65])	0.60
Gastrocnemius lateralis	19.82 – (0.05 × Max [0,cad – 80]) + (0.17 × Max [0,cad – 120]) – (0.09 × Max [0,torque – 28.65])	0.82
Soleus	20.10 + (0.08 × Max [0,28.65 – torque])	0.13
Gastrocnemius medialis	19.18 + (0.05 × Max [0,cad – 80]) + (0.08 × Max [0,120 – cad]) – (0.21 × Max [0,torque – 28.65])	0.77
Vastus lateralis	18.64 + (0.81 × Max [0,80 – cad]) + (0.04 × Max [0,cad – 80]) – (0.11 × Max [0,torque – 28.65])	0.95
Rectus femoris	14.75 + (0.12 × Max [0,cad – 80]) + (0.25 × Max [0,120 – cad]) + (0.003 × Max [0,1909.86 – cad×torque])	0.89
Vastus medialis	20.27 + (0.61 × Max [0,80 – cad])	0.94
Biceps femoris	19.61 + (0.08 × Max [0,100 – cad]) + (0.06 × Max [0,cad – 120]) + (0.18 × Max [0,23.87 – torque])	0.52
Semitendinosus	19.42 + (0.05 × Max [0,80 – cad]) + (0.13 × Max [0,28.65 – torque])	0.29
Gluteus maximus	23.96 + (0.26 × Max [0,80 – cad]) + (0.13 × Max [0,cad – 120]) – (0.002 × Max [0,cad×torque – 1909.86])	0.80

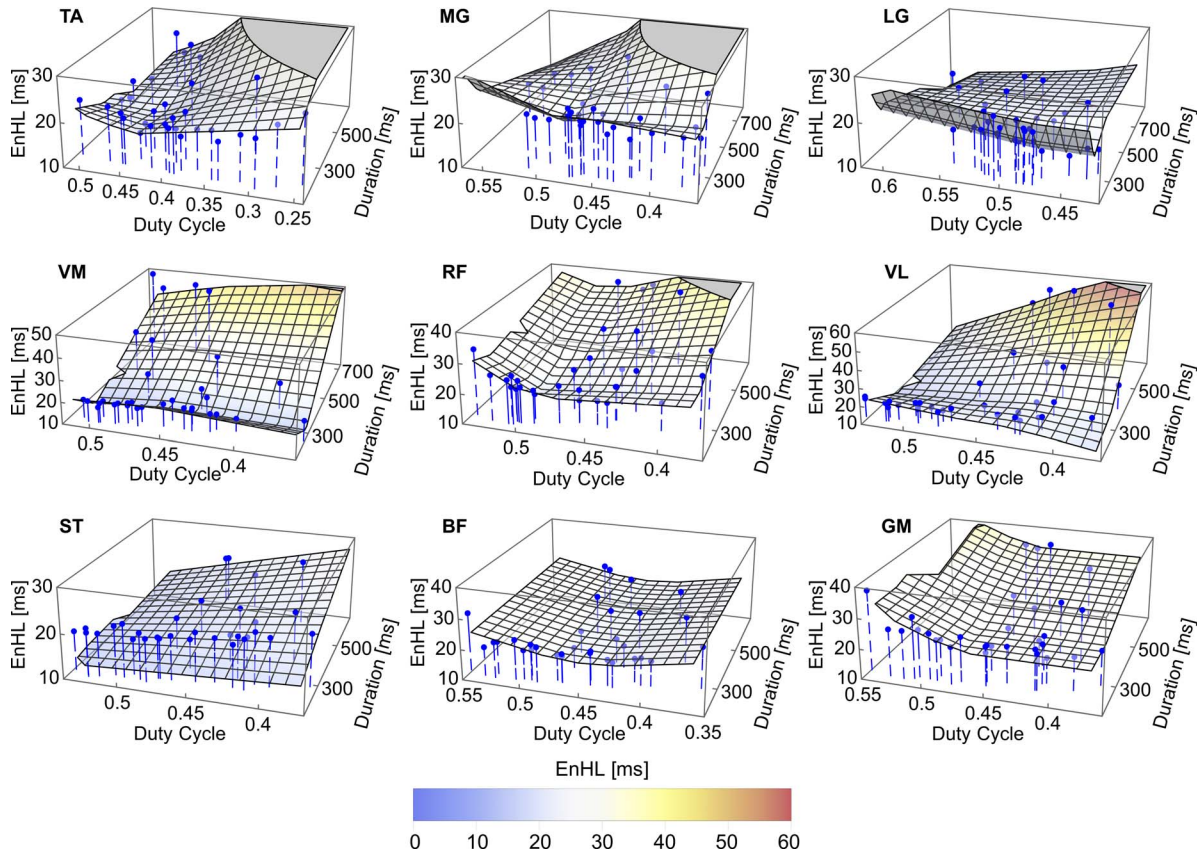

FIGURE 4—EnHL values for excitation patterns (*blue points*) of individual muscles as a function of excitation duration and duty cycle. The overlaid surface represents the excitation pattern EnHL values predicted as a function of excitation duration and duty cycle by MARS analysis. Equations for the surface and associated goodness of fit values are provided in Table 3. See Supplemental Digital Content 5 for animations of the graphics rotating through different viewpoints, http://links.lww.com/MSS/B708.

in Fig. 4 providing multiple perspectives of the 3D space, http://links.lww.com/MSS/B708), and the results of the MARS analysis of these data in Table 3. The relationships between EnHL and these excitation burst parameters showed a greater range of patterns across the muscles studied, than that seen when cycling condition was assessed. Longer EnHL (fewer fluctuations/greater persistence in structure) were associated with longer duty cycles (>0.5) and with both long and short excitation burst durations. The MARS analysis identified a hinge function associated with burst duration in all muscles except BF. The hinge points ranged from 235 ms (LG) to 344 ms (MG) and occurred for pedaling at 80 to 120 rpm. A hinge function related to duty cycle occurred in all muscles except ST, with values ranging between 0.43 (TA, BF) and 0.49 (RF).

DISCUSSION

In agreement with our predictions, muscle coordination became more persistent at cadences up to 120 rpm, indicated by increasing EnHL values for the loading scores of PCI and PCII. Changes in EnHL at the level of the individual muscles differed from the changes in muscle coordination EnHL, with longer EnHL occurring at the slowest (<80 rpm) and fastest

TABLE 3. Details of the MARS model of EnHL as a function of excitation duration (BD) and duty cycle (DC), in each of the 10 lower leg muscles analyzed.

Muscle	MARS Model	Model Fit (r^2)
Tibialis anterior	47.06 – (0.23 × BD × DC) – (0.09 × Max [0,294.2 – BD]) + (0.11 × Max [0,BD – 294.25]) + (75.98 × Max [0,DC – 0.43])	0.57
Gastrocnemius lateralis	17.06 + (0.11 × Max [0,235 – BD]) + (0.03 × Max [0,BD – 235]) + (29.92 × Max [0,dc – 0.48]) – (0.07 × Max [0,BD×DC – 163.85])	0.84
Soleus	No Fit	—
Gastrocnemius medialis	58.69 – (0.33 × BD × DC) – (0.11 × Max [0,244 – BD]) + (0.17 × Max [0,BD – 244]) – (65.95 × Max [0,0.464756 – DC]) + (134.73 × Max [0,DC – 0.48])	0.83
Vastus lateralis	133.67 – (0.82 × BD × DC) – (0.35 × Max [0,298.5 – BD]) + (0.46 × Max [0,BD – 298.5]) – (95.5 × Max [0,DC – 0.43]) – (254.72 × Max [0,0.46 – DC]) + (293.69 × Max [0,DC – 0.46])	0.82
Rectus femoris	45.04 – (0.20 × BD ×DC) – (0.07 × Max [0,254.75 – BD]) + (0.13 × Max [0,BD – 254.75]) + (264.27 × Max [0,DC – 0.49])	0.99
Vastus medialis	38.26 – (0.19 × BD × DC) + (0.16 × Max [0,BD – 283.13]) – (63.23 × Max [0,0.46 – DC])	0.94
Biceps femoris	21.17 + (66.72 × Max [0,0.43 – DC]) + (70.38times; ×times; Max [0,DC – 0.47])	0.39
Semitendinosus	18.49 + (0.06times; × Max [BD – 304.5]) + (0.09 × MAX [0,128.16 – BD × DC]) – (0.11 × MAX [0,BD × DC – 128.16])	0.56
Gluteus maximus	23.59 + (0.03 × Max [0,BD – 300]) + (149.59 × 23`Max [0,DC – 0.47])	0.73

(>120 rpm) cadences. These findings indicate that, within the trained cyclists studied, changes in the structure of individual muscle excitation can occur even when changes in coordination are more limited.

The range of EnHL values found for the individual muscles is strikingly similar to those predicted from simulated, synthetic EMG signals (28) and reported for experimental data from humans cycling (29) and rats running on a treadmill (28). Similar features of EMG structure are, therefore, apparent across the range of mechanical demands, muscles, and species studied to date. Equally, the EnHL for the muscle coordination patterns are similar to those previously reported for a range of cycling conditions (25,29). It has been previously shown that excitation duration and duty cycle change in a complex and nonlinear manner as a function of cycling cadence and power output (2). The results here show that, as with instantaneous measures (2), features of the EMG signal structure also change in a nonlinear manner with cycling task demand. For both individual muscles and muscle coordination 80 and 120 rpm were critical cadences at which hinge points in the EnHL relations occurred.

Longer EnHL indicate that signal structure persisted over longer time periods, representing fewer patterns of the individual muscle excitations or muscle coordination. Longer EnHL are an indication of the availability of fewer solutions that meet the task demands within the system. The results here, therefore, indicate that at cadences slower than 80 rpm and faster than 120 rpm the majority of the limb muscles studied may have fewer fluctuations in the motor unit recruitment or firing characteristics that contribute to the application of force at the pedal. Particularly for the faster cadences, this fits with preferential recruitment of faster motor unit populations (i.e., fewer motor unit populations recruited) (13,14) and an increase in the ineffective forces delivered to the pedals (2) that has previously been shown.

The majority of the muscles in which 120 rpm was identified as a hinge point, above which longer EnHL occurred (MG, LG, RF, BF, Gmax), are biarticular and active at the top or bottom of the pedal cycle. Muscle coordination across these portions of the pedal cycle is important for mechanical efficiency (2) and, as such, limitations in maximum power output at faster cadences may be more related to challenges in orientating and transferring muscle forces rather than generation of force itself. The EnHL of VM and VL, reached a minimum by 80 rpm and did not change across the faster cadences studied (Fig. 3, Supplemental Digital Content 3 animated rotation of plots in Fig. 3 providing multiple perspectives of the 3D space, http://links.lww.com/MSS/B706, Supplemental Digital Content 4 animated rotation of data in Fig. 3 including interquartile ranges of these data, http://links.lww.com/MSS/B707). This indicates that motor unit recruitment and firing characteristics within these muscles were able to provide a consistent number of solutions solving the demands of pedaling across the conditions studied and providing further evidence that these two muscles act mainly as power producers during cycling.

At cadences faster than 120 rpm the timescale over which structure persisted in the main muscle coordination patterns remained approximately constant (Fig. 2, Supplemental Digital Content 1 animated rotation of plots in Fig. 2 providing multiple perspectives of the 3D space, http://links.lww.com/MSS/B704; Supplemental Digital Content 2 animated rotation of data in Fig. 2, including interquartile ranges of these data, http://links.lww.com/MSS/B705). The EnHL of the individual muscles, however, showed a tendency for increasing EnHL from this point, indicating that although the patterns in muscle coordination had consistent structure persistence, the structure of individual muscle excitations were still changing (Table 2, Fig. 3). Therefore, a stable pattern of coordination across multiple muscles does not indicate that each individual muscle contributes the same pattern of behavior across movement cycles. Equally, these results indicate that pedaling cadence (or pedal cycle duration) predominantly limits the solutions available at the level of muscle coordination. This could suggest some form of tuning of neural command signals to individual muscles, as has previously been reported for a range of locomotor activities in cats (36,37). Such tuning could optimize muscle recruitment to exploit differences in morphology (e.g., number joints spanned, fascicle architecture) and/or physiology (e.g., fiber type proportions (15,38,39)) to optimize some feature of task performance (e.g., minimizing energy expenditure (18)) and accommodate small cycle-to-cycle perturbations or variability.

So, why might 120 rpm be such a critical cadence? In the motor control literature Craik (40) and Vince (41) have shown that discrete movements could be made at a maximum frequency of two to three actions per second, above which mutual interference and loss of accuracy occurs. At 120 rpm, cycle durations are ~500 ms, and activation durations are below 200 ms (2). Therefore, at this cadence, adjustments could be made on a cycle-to-cycle basis (i.e., within pedal cycle adjustments); however, at faster cadences, adjustments may only be possible across several pedal cycles. Indeed cadences of 120 to 140 rpm have previously been suggested to provide a critical limit to the duration of muscle excitation and subsequent deterioration in muscle coordination (2). These limits have previously been understood within the context of power producing capabilities of skeletal muscle fibers at different operating velocities (15) and limitations of activation-deactivation capabilities (2). The evidence presented here shows that the intrinsic structure of muscle excitation and coordination patterns is also affected. Indeed, when EnHL in individual muscles was assessed as a function of excitation duration and duty cycle, excitation durations shorter than 304.5 ms were associated with an increase in EnHL across all muscles except BF (Table 3, Fig. 4). Cycling (particularly in a laboratory setting with well-trained individuals) probably presents predictable stimuli where response rates faster than those reported by Craik (40) and Vince (41) are likely to occur. However, the results presented here strongly indicate that factors related to the status of the central and peripheral nervous systems (e.g., distribution of excitatory and inhibitory presynaptic sources) may also

influence muscle excitation and coordination and impact power output from the limb.

CONCLUSIONS

Changes in EnHL at the level of the individual muscles and multi-muscle coordination indicate 120 rpm is a cadence at which the intrinsic structure of muscle excitation and coordination patterns alters. Across the faster cadences where muscle coordination patterns are consistent, changes in the solutions available within individual muscles are still occurring. Whether this is a skill learned through training, and hence, only demonstrated by experienced cyclists (such as those studied here), or whether it is a general feature of motor control that can be found in untrained cyclists and during different locomotor activities (e.g., running, swimming) is not known and warrants further investigation.

Cadences of 120 to 140 rpm have previously been suggested to provide a critical limit to excitation duration (2). Here, excitation durations shorter than 304.5 ms were associated with an increase in EnHL across all muscles except BF (Table 3, Fig. 4), suggesting a greater challenge to the motor control system that could impact maximum power output at cadences above 120 rpm. Changes in the solutions available between pedaling cadences were particularly evident in biarticular muscles, which are likely responsible for orientation and transfer of forces to the pedals. This suggests the time available to coordinate orientation and transfer of forces through the neuromuscular system to the pedals may be key for power production at faster cadences in trained cyclists. Consequently, the importance of muscle coordination at the top and bottom of the pedal cycle could be an important focus for improving cycling performance, particularly in athletes aiming to complete shorter distance, power based events.

There are no professional relationships with companies or manufacturers to disclose for all authors.

This research was supported by the Natural Sciences and Engineering Research Council of Canada (NSERC) Discovery Grant to J. M. Wakeling. O. M. Blake was supported by an NSERC Vanier Scholarship. The results of the present study do not constitute endorsement by the American College of Sports Medicine.

The authors declare that the results of the study are presented clearly, honestly, and without fabrication, falsification, or inappropriate data manipulation.

REFERENCES

1. Martin JC, Nichols JA. Simulated work loops predict maximal human cycling power. *J Exp Biol*. 2018;221(Pt 13).
2. Blake OM, Wakeling JM. Muscle coordination limits efficiency and power output of human limb movement under a wide range of mechanical demands. *J Neurophysiol*. 2015;114(6): 3283–95.
3. Takaishi T, Yasuda Y, Ono T, Moritani T. Optimal pedaling rate estimated from neuromuscular fatigue for cyclists. *Med Sci Sports Exerc*. 1996;28(12):1492–7.
4. Neptune RR, Hull ML. A theoretical analysis of preferred pedaling rate selection in endurance cycling. *J Biomech*. 1999;32(4): 409–15.
5. Marsh AP, Martin PE. Effect of cycling experience, aerobic power, and power output on preferred and most economical cycling cadences. *Med Sci Sports Exerc*. 1997;29(9):1225–32.
6. Marsh AP, Martin PE. The association between cycling experience and preferred and most economical cadences. *Med Sci Sports Exerc*. 1993;25(11):1269–74.
7. Dorel S, Couturier A, Lacour JR, Vandewalle H, Hautier C, Hug F. Force–velocity relationship in cycling revisited: benefit of two-dimensional pedal forces analysis. *Med Sci Sports Exerc*. 2010; 42(6):1174–83.
8. Beelen A, Sargeant AJ. Effect of fatigue on maximal power output at different contraction velocities in humans. *J Appl Physiol (1985)*. 1991;71(6):2332–7.
9. Samozino P, Horvais N, Hintzy F. Why does power output decrease at high pedaling rates during sprint cycling? *Med Sci Sports Exerc*. 2007;39(4):680–7.
10. Hautier CA, Linossier MT, Belli A, Lacour JR, Arsac LM. Optimal velocity for maximal power production in non-isokinetic cycling is related to muscle fibre type composition. *Eur J Appl Physiol Occup Physiol*. 1996;74(1–2):114–8.
11. Jeukendrup AE, Craig NP, Hawley JA. The bioenergetics of world class cycling. *J Sci Med Sport*. 2000;3(4):414–33.
12. MacIntosh BR, Neptune RR, Horton JF. Cadence, power, and muscle activation in cycle ergometry. *Med Sci Sports Exerc*. 2000;32(7):1281–7.
13. Wakeling JM, Uehli K, Rozitis AI. Muscle fibre recruitment can respond to the mechanics of the muscle contraction. *J R Soc Interface*. 2006;3(9):533–44.
14. Wakeling JM, Horn T. Neuromechanics of muscle synergies during cycling. *J Neurophysiol*. 2009;101(2):843–54.
15. Blake OM, Wakeling JM. Early deactivation of slower muscle fibres at high movement frequencies. *J Exp Biol*. 2014;217(Pt 19):3528–34.
16. Dick TJM, Biewener AA, Wakeling JM. Comparison of human gastrocnemius forces predicted by Hill-type muscle models and estimated from ultrasound images. *J Exp Biol*. 2017;220(Pt 9): 1643–53.
17. Lai AKM, Arnold AS, Biewener AA, Dick TJM, Wakeling JM. Does a two-element muscle model offer advantages when estimating ankle plantar flexor forces during human cycling? *J Biomech*. 2018; 68:6–13.
18. Lai AKM, Biewener AA, Wakeling JM. Metabolic cost underlies task-dependent variations in motor unit recruitment. *J R Soc Interface*. 2018;15(148).
19. Muller H, Sternad D. Motor learning: changes in the structure of variability in a redundant task. *Adv Exp Med Biol*. 2009;629:439–56.
20. Hoffer JA, Loeb GE, Sugano N, Marks WB, O'Donovan MJ, Pratt CA. Cat hindlimb motoneurons during locomotion. III. Functional segregation in sartorius. *J Neurophysiol*. 1987;57(2):554–62.
21. de Luca CJ, LeFever RS, McCue MP, Xenakis AP. Control scheme governing concurrently active human motor units during voluntary contractions. *J Physiol*. 1982;329:129–42.
22. Vieira TM, Minetto MA, Hodson-Tole EF, Botter A. How much does the human medial gastrocnemius muscle contribute to ankle torques outside the sagittal plane? *Hum Mov Sci*. 2013; 32(4):753–67.
23. Herrmann U, Flanders M. Directional tuning of single motor units. *J Neurosci*. 1998;18(20):8402–16.
24. Hodson-Tole EF, Loram ID, Vieira TM. Myoelectric activity along human gastrocnemius medialis: different spatial distributions of postural and electrically elicited surface potentials. *J Electromyogr Kinesiol*. 2013;23(1):43–50.

25. Enders H, Von Tscharner V, Nigg BM. Neuromuscular strategies during cycling at different muscular demands. *Med Sci Sports Exerc*. 2015;47(7):1450–9.
26. Federolf P, Zandiyeh P, von Tscharner V. Time scale dependence of the center of pressure entropy: what characteristics of the neuromuscular postural control system influence stabilographic entropic half-life? *Exp Brain Res*. 2015;233(12):3507–15.
27. Zandiyeh P, von Tscharner V. Reshape scale method: a novel multi scale entropic analysis approach. *Phys A: Stat Mech Applic*. 2013; 392(24):6265–72.
28. Hodson-Tole EF, Wakeling JM. Movement complexity and neuromechanical factors affect the entropic half-life of myoelectric signals. *Front Physiol*. 2017;8:679.
29. Wakeling JM, Hodson-Tole E. How do the mechanical demands of cycling affect the information content of the EMG? *Med Sci Sports Exerc*. 2018;50(12):2518–25.
30. von Tscharner V. Intensity analysis in time-frequency space of surface myoelectric signals by wavelets of specified resolution. *J Electromyogr Kinesiol*. 2000;10(6):433–45.
31. Goldberger AL, Amaral LA, Glass L, et al. PhysioBank, PhysioToolkit, and PhysioNet: components of a new research resource for complex physiologic signals. *Circulation*. 2000;101(23):E215–20.
32. Richman JS, Moorman JR. Physiological time-series analysis using approximate entropy and sample entropy. *Am J Physiol Heart Circ Physiol*. 2000;278(6):H2039–49.
33. Ramsay JO, Silverman BW. *Applied Functional Data Analysis: Methods and Case Studies*. Springer-Verlag; 1997.
34. Friedman JH. Multivariate adaptive regression splines. *Ann Statist*. 1991;19(1):1–67.
35. Milborrow S. (Derived from mda:mars by T. Hastie and R. Tibshirani) Earth: Multivariate Adaptive Regression Splines. In: R package; 2011.
36. Degtyarenko AM, Simon ES, Norden-Krichmar T, Burke RE. Modulation of oligosynaptic cutaneous and muscle afferent reflex pathways during fictive locomotion and scratching in the cat. *J Neurophysiol*. 1998;79(1):447–63.
37. O'Donovan MJ, Pinter MJ, Dum RP, Burke RE. Actions of FDL and FHL muscles in intact cats: functional dissociation between anatomical synergists. *J Neurophysiol*. 1982;47(6):1126–43.
38. Hodson-Tole EF, Wakeling JM. Motor unit recruitment patterns 1: responses to changes in locomotor velocity and incline. *J Exp Biol*. 2008;211(12):1882–92.
39. Hodson-Tole EF, Wakeling JM. Variations in motor unit recruitment patterns occur within and between muscles in the running rat (*Rattus norvegicus*). *J Exp Biol*. 2007;210(13):2333–45.
40. Craik KJ. Theory of the human operator in control systems; the operator as an engineering system. *Br J Psychol Gen Sect*. 1947;38(Pt 2): 56–61.
41. Vince MA. The intermittency of control movements and the psychological refractory period. *Br J Psychol Gen Sect*. 1948; 38(Pt 3):149–57.